LETTER

ACS chemical biology

Regulation of Alkyl-dihydrothiazole-carboxylates (ATCs) by Iron and the Pyochelin Gene Cluster in *Pseudomonas aeruginosa*

Nawaporn Vinayavekhin and Alan Saghatelian*

Department of Chemistry and Chemical Biology, Harvard University, Cambridge, Massachusetts 02138

ABSTRACT Using the pyochelin (*pch*) gene cluster as an example, we demonstrate the utility of untargeted metabolomics in the discovery and characterization of secondary metabolites regulated by biosynthetic gene clusters. Comparison of the extracellular metabolomes of *pch* gene cluster mutants to the wild-type *Pseudomonas aeruginosa* (strain PA 14) identified 198 ions regulated by the *pch* genes. In addition to known metabolites, we characterized the structure of a pair of novel metabolites regulated by the *pch* gene cluster as 2-alkyl-4,5-dihydrothiazole-4-carboxylates (ATCs), using a combination of mass spectrometry, chemical synthesis, and stable isotope labeling. Subsequent assays revealed that ATCs bind iron and are regulated by iron levels in the media in a similar fashion as other metabolites associated with the *pch* gene cluster. Further genetic complementation and overexpression analyses of the *pch* genes revealed ATC production to be dependent on the *pchE* gene in the *pch* gene cluster. Overall, these studies highlight the ability of untargeted metabolomics to reveal regulatory connections between gene clusters and secondary metabolites, including novel metabolites.

The biosynthesis of natural products typically occurs through an iterative series of enzymatic reactions that generates sophisticated molecular structures from simple pools of starting materials (*1, 2*), such as CoA esters and activated amino acids. Since natural product biosynthetic enzymes are required to work in concert, they are co-expressed. In addition, the genes that encode biosynthetic enzymes are often found in proximity to each other on genomes as gene clusters. The sequencing of bacterial genomes, such as the *Streptomyces coelicolor* A3 genome (*3*), has begun to reveal biosynthetic gene clusters that code for secondary metabolites of unknown structure. These uncharacterized gene clusters are referred to as "orphan" or "cryptic" gene clusters to indicate the lack of knowledge about the metabolites regulated by these genes. We reasoned that a liquid chromatography−mass spectrometry (LC−MS)-based untargeted metabolomics approach could accelerate the discovery of natural products regulated by biosynthetic gene clusters, including biosynthetic products, by measuring changes in the metabolome as a function of the expression of genes within a cluster. Here, we demonstrate this approach by combining untargeted metabolomics with genetics to identify secondary metabolites regulated by the pyochelin (*pch*) gene cluster in *Pseudomonas aeruginosa* (strain PA14).

Pyochelin is one of the principle siderophores that *P. aeruginosa* uses for the acquisition of iron from the surrounding environment (*4*). The *pch* gene cluster encodes a nonribosomal peptide synthase that combines one molecule of salicylate with two molecules of cysteine to form pyochelin (*5–8*). Within the *pch* gene cluster the enzymes encoded by the *pchD*, *pchE*, *pchF*, and *pchG* genes are responsible for the assembly of the pyochelin core (Figure 1). During the biosynthesis of pyochelin, PchD generates an acyl adenylate from salicylic acid, which is then used by PchE to conjugate and cyclize a cysteine to form a thiazoline ring. Interestingly, the PchF-mediated production of the second thiazoline ring, reduction of this ring to a thiazolidine by the PchG, and SAM-dependent N-methylation of this intermediate thaizolidine to afford pyochelin all occur *via* an acyl-*S*-enzyme intermediate (*6*). In fact, both the PchE and PchF proteins operate through an enzyme-bound acyl-*S*-enzyme intermediate (Figure 1), but hydrolysis of biosynthetic intermediates does occur at some level since 4,5-dihydro-2-(2-hydroxyphenyl)-4-thiazolecarboxylic acid (HPTn-COOH) has been detected *in vivo* (*8*) and *in vitro* (*5, 6*). Additionally, a thioesterase encoded by the *pchC* gene can regulate the amount of pyochelin generated by this pathway (~3-fold) by removing mischarged amino acids from PchE and PchF, which increases the flux through the pathway (*7*). By integrating untargeted metabolomics with genetic mutants that target some of the *pch* genes, we reveal the full spectrum of secondary metabolites regulated by this gene cluster to be larger than previously anticipated.

Mutant PA14 strains targeting *pchC*, *pchD*, *pchE*, and *pchF* genes were obtained

*Corresponding author, saghatelian@chemistry.harvard.edu.

Received for review December 20, 2008 and accepted June 28, 2009.

Published online June 29, 2009

10.1021/cb900075n CCC: $40.75

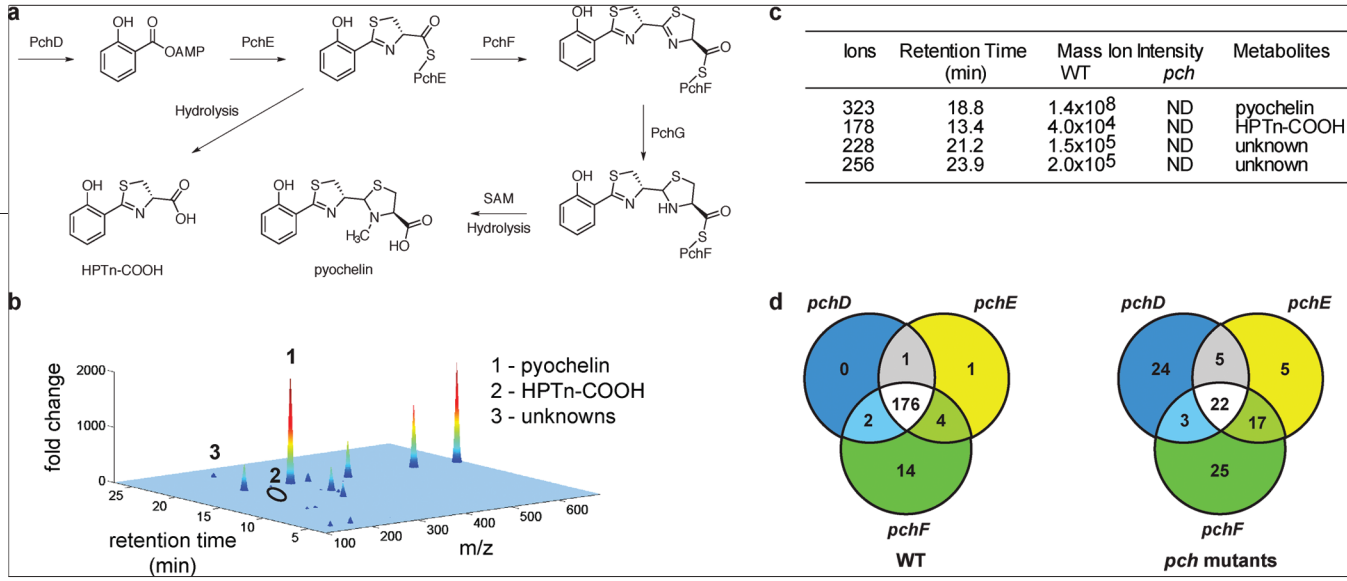

Figure 1. Pyochelin biosynthesis and untargeted metabolomics of *P. aeruginosa pch* mutants. a) The key steps in pyochelin biosynthesis mediated by the enzymes encoded by the *pchD*, *pchE*, *pchF*, and *pchG* genes of the *pch* gene cluster (*5, 6*). b) Untargeted metabolomics and comparison of the extracellular metabolome from *P. aeruginosa* strains where mass ion intensity ratios (WT/*pchD*) of metabolites are presented on a three-dimensional surface plot. These ratios are plotted over a mass range of 100−690 Da and liquid chromatography retention times of 3−27 min (plot shown for negative ionization mode), and peaks represent those ions elevated in the WT sample. WT metabolomes possessed highly elevated levels of (1) pyochelin, (2) HPTn-COOH, as well as a group of (3) unidentified ions. c) Relative levels of the different ions with respect to pyochelin based on the absolute mass ion intensities (ND = not detected). d) A Venn diagram showing the total number of significantly ($p < 0.05$, Student's *t* test, 3-fold or more) changing ions (positive and negative mode) elevated in WT (left) or *pch* mutant (right) strains.

from a previously generated transposon insertion mutant library (*9*) (see Methods for mutant identification numbers). Because two of the metabolic products of the *pch* gene cluster, pyochelin and HPTn-COOH, are secreted into the media, we focused our attention on differences in the extracellular metabolome in this study. Overnight cultures (3 mL) of wild-type (WT) and mutant PA14 strains were used to inoculate larger cultures (25 mL), which were then grown to early stationary phase ($OD_{600} = 1.7$). There were no apparent differences in the growth rate between the different mutant strains and WT PA14. After the cells reached the early stationary phase, cells were pelleted, and the supernatant was extracted using organic solvent to isolate any lipophilic small molecule metabolites, such as pyochelin. This extract was then concentrated and used directly for analysis by our LC−MS-based untargeted metabolomics platform. As expected, pyochelin levels were lower in the *pchC* mutant strain and completely absent from the *pchD*, *pchE*, and *pchF* mutant strains (Figure 1).

To identify differences in the levels of other metabolites, the untargeted metabolomics data was analyzed using the XCMS (*10*) software package. XCMS identifies changes in metabolite levels between pairs of samples (*e.g.*, *pchD vs* WT, *pchE vs* WT) by aligning peaks within the LC−MS chromatograms, quantifying these peaks using the ion intensity (*i.e.*, area under the curve), and ranking these differences on the basis of statistical significance. The outputs from XCMS are then manually normalized to the OD of the sample and filtered to remove any false positives by setting thresholds for fold change (>3-fold), ion intensities (30,000 counts), and statistical significance (Student's *t* test, *p*-value < 0.05). Because the metabolomics and data analysis are unbiased, each set of pairwise comparisons contained known metabolites, such as pyochelin, as well as ions corresponding to unknown metabolites (Figure 1).

Pairwise comparison of the WT PA14 strain to the *pchE*, *pchD*, and *pchF* mutants identified 231, 233, and 263 significant differences, respectively. Of these differences, 198 ions were regulated in a similar fashion across all three mutants. A majority of these overlapping ions (176 ions) were elevated in the WT sample, and the remaining ions (22 ions) were higher in all three of the mutant samples (Figure 1 and Supporting Information). Although these numbers are larger than anticipated on the basis of known biosynthetic products of *pch* gene cluster, other gene clusters have been shown to directly produce or indirectly regulate the levels of hundreds of metabolites (*11, 12*). As untargeted metabolomics approaches are applied to additional gene clusters, we will discover whether the regulation of a large number of secondary metabolites is a general phenomena.

Using a combination of accurate mass, which provides molecular formulas, and data from *in vitro* reconstitution experiments (*6*) with the *pch* cluster, a number of the ions elevated in the WT sample were thought to be biosynthetic intermediates of the pyochelin pathway. Specifically, we were able to detect HPTn-COOH, 2′-(2-hydroxyphenyl)-4′-thiazolyl-2,4-thiazolinyl-4-carboxylic acid (HPTzTn-COOH) and 4′,5′-dihydro-2′-(2-hydroxyphenyl)-4′-thiazolinyl-2,4-thiazolidyl-4-carboxylic acid (HPTnTd-COOH) (Figure 2). We confirmed the structural assignment of HPTn-COOH by comparison of a synthetic standard to the natural metabolite in the WT sample by co-elution and accurate mass (Figure 2).

Moreover, we gained additional support for the structural assignments of all of these biosynthetic intermediates by growing WT PA14 in the presence of DL-cysteine-3,3-d_2,

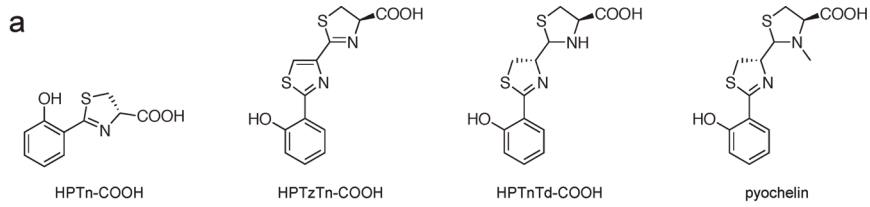

Metabolites	Ions	m/z	Retention Time (min)	Mass Ion Intensity WT	*pch*
HPTn-COOH	$[M - H - CO_2]^-$	178	13.4	4.0×10^4	ND
HPTzTn-COOH	$[M - H]^-$	305	10.3	5.1×10^4	ND
HPTnTd-COOH	$[M - H]^-$	309	17.2	2.6×10^5	ND

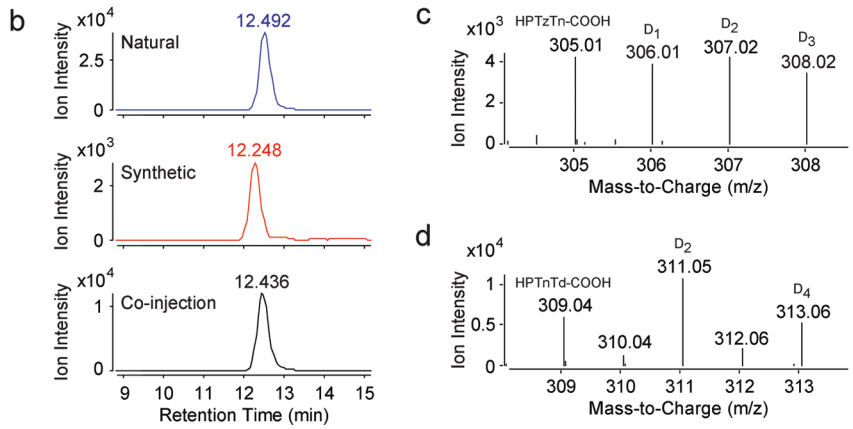

Figure 2. Detection and characterization of known pyochelin biosynthetic intermediates. a) Biosynthetic intermediates from the pyochelin pathway detected in the WT PA14 but not in the *pch* mutant samples. Based on the known steps in pyochelin production, HPTn-COOH results from the premature release of the metabolite from PchE, whereas HPTnTd-COOH is released from PchF, prior to completion of pyochelin biosynthesis. HPTzTn-COOH also results from premature cleavage from PchF followed by an oxidation step. b) The structure of HPTn-COOH was confirmed by co-elution experiments with a synthetic standard. Additional evidence for the assignment of HPTzTn-COOH and HPTnTd-COOH was obtained through stable isotope labeling experiments with WT PA14 grown in the presence of DL-cysteine-3,3-d_2. c) On the basis of the proposed HPTzTn-COOH structure, the incorporation of DL-cysteine-3,3-d_2 into the first ring, second ring, or both rings would result in the addition of a one, two, or three deuteriums and provide the observed isotope pattern. d) Since the HPTnTd-COOH structure is not oxidized, the anticipated isotope pattern would include two or four deuteriums, which is what is observed.

which was added to the media (Figure 2 and Supporting Information). Utilization of isotope-labeled cysteine by the pyochelin biosynthetic pathway should produce deuterated variants of the biosynthetic intermediates, which can easily be detected by mass spectrometry. For example, the isotope pattern for HPTzTn-COOH in samples grown in the presence of DL-cysteine-3,3-d_2 shows the incorporation of a single deuterium, two deuteriums, and three deuteriums, which is the expected frequency for incorporation of isotope-labeled cysteine into the first ring, second ring, and both rings, respectively (Figure 2). The detection of pyochelin intermediates *in vivo* corroborates *in vitro* reconstitution experiments and demonstrates the potential of untargeted metabolomics in helping define the key biosynthetic intermediates in the production of secondary metabolites.

Normally, the loss of enzymatic activity in a biochemical pathway, such as the loss of *pchD*, *pchE*, or *pchF*, would result in the accumulation of substrates leading to elevated levels of intermediates in mutant samples (*13*). In this case with the *pch* gene cluster, however, the intermediates are elevated in the WT sample. The observation of elevated pyochelin intermediates in the WT samples is explained by a known positive feedback loop (*8*) that requires pyochelin for the expression of *pchDCGA* and *pchEFGHI* operons. As a result of this feedback loop, the absence of pyochelin in the mutant strains results in a decreased expression of all *pch* genes, which results in lower levels of all of the pyochelin biosynthetic intermediates in the mutant strains when compared to the WT strain.

We scanned the remaining WT elevated ions in search of novel metabolites that are regulated in a similar fashion as pyochelin and HPTn-COOH (*i.e.*, co-regulated) and found two promising candidates with *m/z* of 228 and 256 for structural elucidation (Figure 1). Like pyochelin and HPTn-COOH, these ions were elevated in WT samples and not detectable in any of the mutant samples (Figure 1 and Supporting Information). The accurate mass of these ions provided molecular formulas of $C_{11}H_{18}NO_2S$ (228 ion) and $C_{13}H_{22}NO_2S$ (256 ion), which revealed that these metabolites shared a conserved heteroatom region and a variable hydrocarbon group. The difference in the hydrocarbon region was equivalent to two methylene (CH_2) units, which is reminiscent of the pattern seen with fatty acids, and one option might be that these two metabolites contain acyl chains. The surprising hypothesis that the *pch* gene cluster is regulating a fatty

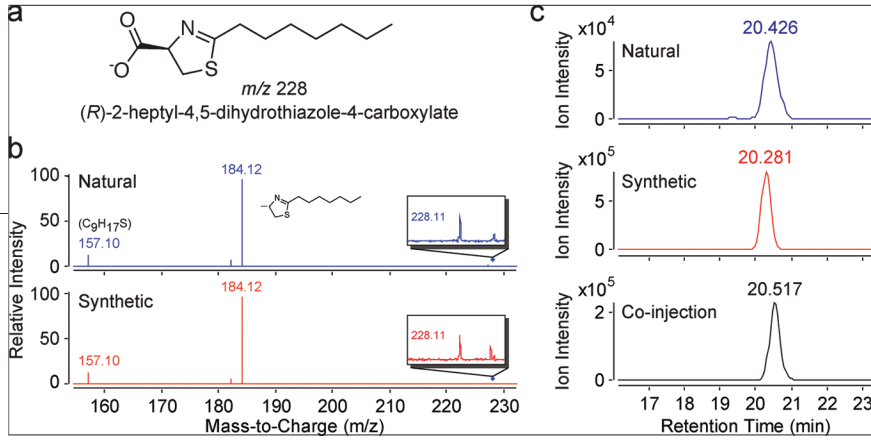

Figure 3. Characterization of the unknown *m/z* 228 ion by chemical synthesis and LC–MS. a) The proposed structure of the *m/z* 228 ion as 2-heptyl-4,5-dihydrothiazole-4-carboxylate (ATC). Comparison of the natural metabolite to the synthetic standard by (b) co-elution and (c) MS/MS confirmed the assignment of the *m/z* 228 ion as the previously unknown 2-heptyl-4,5-dihydrothiazole-4-carboxylate metabolite.

acylated secondary metabolite prompted us to structurally characterize these ions.

More specifically, we believed that these ions were condensation products of octanoic and decanoic acid with cysteine to afford 2-heptyl-4,5-dihydrothiazole-4-carboxylate (228 ion) and 2-nonyl-4,5-dihydrothiazole-4-carboxylate (256 ion) (Figure 3). We set out to confirm the structure of these 2-alkyl-4,5-dihydrothiazole-4-carboxylates (ATCs) by chemical synthesis of the 2-heptyl-4,5-dihydrothiazole-4-carboxylate and the 2-nonyl-4,5-dihydrothiazole-4-carboxylate metabolites (Supporting Information). Comparison of the synthetic standards with the natural compound by LC–MS demonstrated that the synthetic compounds and the natural metabolites co-eluted and gave identical accurate masses (Figure 3 and Supporting Information). In addition, fragmentation spectra for the synthetic and natural compounds were a match to establish the structure of the 228 ion as 2-heptyl-4,5-dihydrothiazole-4-carboxylate and the 256 ion as 2-nonyl-4,5-dihydrothiazole-4-carboxylate (Figure 3 and Supporting Information). In addition, stable isotope labeling with DL-cysteine-3,3-d_2 resulted in the production of deuterated cysteine versions of these metabolites in WT samples (Supplementary Figure 6).

Next, we set out to identify the absolute stereochemistry of the ATCs by generating a diastereomeric amide with the chiral amine (1*S*,2*S*)-(+)-2-amino-1-(4-nitrophenyl)-1,3-propanediol (ANPAD) (Supporting Information). Incubation of ANPAD with the natural metabolite extract in the presence of *N*-hydroxybenzotriazole (HOBt) and 1-ethyl-3-(3-dimethylaminopropyl) carbodiimide hydrochloride (EDC) resulted in the formation of ANPAD amide derivative of 2-heptyl-4,5-dihydrothiazole-4-carboxylate. In parallel, we also prepared ANPAD amides of (*R*)- and (*S*)-2-heptyl-4,5-dihydrothiazole-4-carboxylate by chemical synthesis starting with (*R*)- and (*S*)-cysteine. Comparison of the natural diastereomer to our synthetic derivatives using LC–MS retention times revealed that the absolute stereochemistry of the natural metabolite is (*R*)-2-heptyl-4,5-dihydrothiazole-4-carboxylate (Supporting Information). To our knowledge this is the first description of these metabolites as natural products produced by any organism.

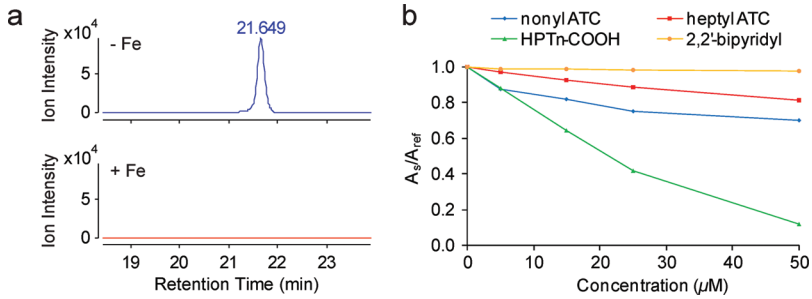

Figure 4. Iron regulation of ATC levels and ATC binding of iron. a) Ion chromatogram of 2-heptyl-4,5-dihydrothiazole-4-carboxylate (*m/z* 228) in iron-deficient (top) and iron-replete (bottom) M9 media showed the absence and regulation of the ATCs in the presence of iron in the media. (b) The chrome azurol S (CAS) assay for testing the iron affinity of 2-nonyl-4,5-dihydrothiazole-4-carboxylate and 2-heptyl-4,5-dihydrothiazole-4-carboxylate, compared to that of HPTn-COOH and 2,2′-bipyridyl. The CAS assay uses an iron–dye complex which changes color from blue to orange on loss of iron, resulting in the lower absorbance reading at 630 nm. The graph was plotted as the relative absorbance at 630 nm (A_s/A_{ref}) *versus* the concentrations of samples.

We then looked at the regulation and chemical properties of the ATCs. First, we tested whether the addition of iron to the media of the WT strain regulates ATC levels. Addition of iron ($FeCl_3$) to the WT PA14 strain resulted in the disappearance of the ATCs (Figure 4) from the media. Pyochelin was not detected under these conditions as expected (Supporting Information). Thus, the ATCs and pyochelin are co-regulated by iron as well as by the *pch* gene cluster. On the basis of the regulation of the ATCs with iron and their structure, we suspected that the ATCs might be able to bind iron as well.

We tested this by comparison of the iron binding ability of 2-nonyl-4,5-dihydrothiazole-4-carboxylate, 2-heptyl-4,5-dihydrothiazole-4-carboxylate, HPTn-COOH, and 2,2′-bipyridyl (bipy) using the chrome azurol S (CAS) assay (*14*), which measures the displacement of a chromophore from iron upon exposure to an iron chelator. We would have liked to include pyochelin as well but could not purify pyochelin in sufficient purity or quantity for these experiments. In these assays, bipy (*15*) and HPTn-COOH, both known iron chelators, served as a positive control. Analysis of the ATCs revealed that these metabolites are better iron binders than bipy but not as good as HPTn-COOH (Figure 4 and Supporting Information). The ability of the ATCs to bind to iron provides a functional connection between ATCs and other natural products regu-

TABLE 1. Effects of the *pchDCBA* and *pchEFG* genes on the production of pyochelin, HPTn-COOH, and ATCs in the *pchD* mutant

Plasmid	Genes carried	Pyochelin	HPTn-COOH	ATCs
pME9623	*entDpchDCBA*	yes	yes	yes
pME6482	*pchE*	no	no	yes
pME6486	*pchEF*	no	no	yes
pME6488	*pchEFG*	no	no	yes

lated by the *pch* cluster (pyochelin and HPTn-COOH).

As with any discovery-based approach, the identification of the ATCs raises new questions, including how the ATCs are regulated by the *pch* gene cluster. To gain additional support for the direct regulation of the ATCs by the proteins encoded in the *pch* gene cluster, we performed a complementation experiment. In this experiment we relied on a previously derived plasmid encoding the *pchDCBA* portion of the *pch* gene cluster to complement the *pchD* mutant strain (Table 1) (*16*). Complementation with the *pchDCBA* expressing plasmid rescued the production of pyochelin and HPTn-COOH in the *pchD* mutant strain. Importantly, ATC production was also rescued by this experiment, which supports the notion that the ATCs are regulated by the *pch* gene cluster (Table 1 and Figure 5). Of course, these experiments do not indicate whether ATC production is directly regulated by genes within the pyochelin gene cluster or an indirect consequence of the production of pyochelin.

In an attempt to distinguish between these two mechanisms, we looked at the effect of different genes within the pyochelin cluster on the production of pyochelin, HPTn-COOH, and ATCs. Our hypothesis is that the ATCs are biosynthetic products of the *pch* gene cluster. The rationale for this model is based on the co-regulation of ATCs and pyochelin, as well as the thiazoline ring found in both metabolites, which could be derived from similar chemistries and, therefore, the same enzymes. In the case of the ATCs, we believe that the thiazoline ring structure is likely produced by an enzyme-catalyzed condensation of cysteine with an activated fatty acid, such as an fatty acyl adenylate. Importantly, *in vitro* biochemical assays demonstrated that *pchD* is unable to activate fatty acids (Supporting Information), which provided us with a way to decouple pyochelin production from ATC regulation. In the absence of *pchD*, which is responsible for salicylate adenylation, the production of pyochelin is not possible (*6*). Thus, overexpression experiments in the *pchD* mutant background can identify genes responsible for ATC production in the absence of pyochelin and HPTn-COOH, which will not be produced.

Indeed, expression of *pchE* in the *pchD* mutant did not result in the reappearance of pyochelin; however, this experiment did result in the production of the ATCs (Table 1 and Figure 5). First, this experiment conclusively shows that ATC production is not dependent on the presence of pyochelin. Moreover, it is clear that *pchE* expression is sufficient for the production of ATCs. Based on the known biochemistry of PchE, we suspect that this regulation is occurring *via* a biosynthetic mechanism where an activated fatty acid and a cysteine residue are condensed and cyclized by PchE. To our knowledge there is no known enzyme within the pyochelin gene cluster capable of generating activated fatty acids necessary for ATC production. As a result, the more general implication from this experiment is that the ATCs are the result of cross-talk between the pyochelin pathway (*pchE*) and another pathway, which has to be determined, that is generating activated fatty acids (*17, 18*).

In conclusion, by coupling untargeted metabolomics analysis to genetic mutants of a specific gene cluster, we were able to readily identify the full spectrum of secondary metabolites regulated by a cluster, which in this case was larger than anticipated. We identified the structures of a pair of novel metabolites regulated by the *pch*

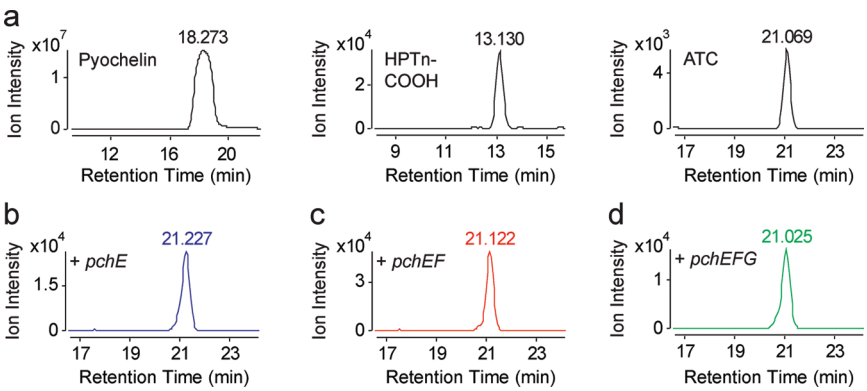

Figure 5. Rescue of ATC production in a *pchD* mutant strain by plasmids harboring portions of the *pch* cluster. a) Ion chromatograms of pyochelin, HPTn-COOH, and 2-heptyl-4,5-dihydrothiazole-4-carboxylate (*m*/*z* 228) after complementation of the *pchD* mutant with a plasmid containing the *pchDCBA* genes. Overexpression of (b) *pchE*, (c) *pchEF*, and (d) *pchEFG* in a *pchD* mutant background rescues the production of 2-heptyl-4,5-dihydrothiazole-4-carboxylate to indicate that *pchE* is sufficient for ATC production.

cluster by mass spectrometry and chemical synthesis as the ATCs. Subsequent experiments identified that the ATCs are regulated by iron and can also bind iron, albeit more weakly than HPTn-COOH. Complementation experiments confirmed the regulation of the ATCs by the *pch* cluster, and overexpression studies revealed that among genes in the *pch* cluster, the *pchE* gene is sufficient for the production of the ATCs. The characterization of *pchE* gene as the sole component of the *pch* cluster necessary for ATC production indicates cross-talk between the *pch* cluster and another, yet to be determined, cluster responsible for making activated fatty acids. More generally, these results point to the importance of studying gene clusters within the context of their natural environments where pathways exist that would not be evident during *in vitro* studies. We anticipate that the increased coverage and rate at which untargeted metabolomics experiments can analyze the metabolome will be extremely useful in biochemical, biosynthetic, and physiological studies in microbiology.

METHODS

Bacterial Strains, Media, and Growth Conditions. Bacterial species and strains used for the global metabolite profiling experiment were derived from the *P. aeruginosa* UCBPP-PA14 (*19*) strain. The PA14 mutants containing the *MAR2xT7* transposon inserted in the *pchC*, *pchD*, *pchE*, and *pchF* genes have mutant identification no. (MID) 54060, 42509, 38966, and 24493, respectively, and both the PA14 wild-type (WT) and mutant strains were generously provided by F. M. Ausubel (Massachusetts General Hospital, Boston, MA). For this study, unless stated otherwise, bacterial strains were grown aerobically at 250 rpm and 37 °C in M9 minimal medium (Difco) supplemented with 0.5% casamino acid (Difco) and 0.2% glucose. For the mutant strains, when applied, gentamicin was added to the medium at 15 μg mL^{-1}. Control experiments show that this antibiotic treatment does not influence metabolites such as the ATCs (Supporting Information).

Verification of PA14 Mutants. PA14 mutant strains (3 mL) were grown overnight at 225 rpm and 37 °C in LB medium (Difco) containing 15 μg mL^{-1} gentamicin. From these cultures, genomic DNA (gDNA) of each strain was isolated and purified using Generation Capture Column kit (Qiagen), according to the manufacturer's instructions. Polymerase chain reaction (PCR) was then performed to amplify the gene region containing the *MAR2xT7* transposon, using the gDNA as a template (see Supporting Information for primers). Subsequently, the PCR products were applied to 0.9% agarose gel, and specific DNA bands were excised under UV light, purified by QIAquick Gel Extraction kit (Qiagen), and submitted for sequencing (GENEWIZ Inc.).

Bacterial Cultures and Extraction. Cultures (3 mL) of PA14 wild-type and mutant strains were grown overnight in M9 medium. The cells were diluted 1000-fold into 25 mL of M9 medium and grown for 9.5 h to early stationary phase (OD_{600} = 1.7). Then, supernatant was collected upon centrifugation of cultures at 3220*g* for 60 min at 4 °C, followed by filtration through a 0.2 μm cellulose acetate membrane. A sample (20 mL) of the filtrate was extracted with a mixture of 10 mL of $CHCl_3$ and 5 mL of MeOH solution (in 11-dram vials), and the mixture was centrifuged at 200*g* for 20 min to separate the organic layer (bottom) from the aqueous layer (top). The organic layer was carefully removed, transferred to another vial, and concentrated under a stream of nitrogen. Samples were stored at −80 °C and dissolved in 200 μL of $CHCl_3$ prior to analysis by LC−MS.

LC−MS of Supernatant Metabolomes. LC−MS analysis was performed using either an Agilent 6220 LC-ESI-TOF instrument or an Agilent 6520 LC-ESI-QTOF instrument. For the LC analysis in the negative ion mode, a Gemini (Phenomenex) C18 column (5 μm, 4.6 mm × 50 mm) was used together with a precolumn (C18, 3.5 μm, 2 mm × 20 mm). Mobile phase A consisted of a 95/5 water/methanol mixture, and mobile phase B was made up of 60/35/5 isopropanol/methanol/water. Both A and B were supplemented with 0.1% ammonium hydroxide as solvent modifiers. The gradient started at 0% B for 5 min at 0.1 mL min^{-1} and then linearly increased to 100% B over the course of 45 min at 0.4 mL min^{-1} followed by an isocratic gradient of 100% B for 8 min at 0.5 mL min^{-1} before equilibration for 7 min at 0.5 mL min^{-1}. The total analysis time, including 5 min at 0.1 mL min^{-1}, was 60 min.

For the LC analysis in the positive ion mode, a Luna (Phenomenex) C5 column (5 μm, 4.6 mm × 50 mm) was used together with a precolumn (C4, 3.5 μm, 2 mm × 20 mm). Mobile phases A and B, as well as the gradient, were the same as that used for the negative ion mode analysis, except that, in this case, both A and B were supplemented with 0.1% formic acid and 5 mM ammonium formate as solvent modifiers. MS analysis was performed with an electrospray ionization (ESI) source. The capillary voltage was set at 3.5 kV and the fragmentor voltage to 100 V. The drying gas temperature was 350 °C, the drying gas flow rate was 10 L min^{-1}, and the nebulizer pressure was 45 psi. For both ionization conditions, data was collected in the profile mode using a mass range of 100−1500 Da, and each run was performed using 50 μL injections of supernatant metabolite extract.

LC−MS Data Analysis. The total ion chromatogram of the following sets of samples was obtained (with 3 experimental replicates for each): (A) PA14 wild-type strain, (B) PA14 *pchC* mutant strain (MID 54060), (C) PA14 *pchD* mutant strain (MID 42509), (D) PA14 *pchE* mutant strain (MID 38966), and (E) PA14 *pchF* mutant strain (MID 24493). The analysis of the resulting total ion chromatograms was performed in two steps: (i) automated data analysis by XCMS (*10*) and (ii) manual statistical analysis, confirmation, and filtering of the XCMS output files. The full details of this analysis can be found in the Supporting Information.

Tandem MS Experiments. MS/MS experiments were performed in the negative ion mode using an Agilent 6520 LC-ESI-QTOF instrument. The tandem MS analysis was performed in the targeted MS/MS mode with 228.10640 or 256.13767 as target mass and narrow (~1.3 amu) as target isolation width. The collision energy was set at 15 V. Data was collected in both the centroid and profile modes using a mass range of 100−1500 Da. The run was performed using 50 μL injection of supernatant metabolite extract from the PA14 wild-type strain as the sample and 5 μL injection of 100 μM sodium (*R*)-2-heptyl-4,5-dihydrothiazole-4-carboxylate or sodium (*R*)-2-nonyl-4,5-dihydrothiazole-4-carboxylate in $CHCl_3$ as the standard.

Coinjection Experiment. Co-injection experiment was performed in the negative ion mode using either an Agilent 6220 LC-ESI-TOF instrument or an Agilent 6520 LC-ESI-QTOF instrument. Both the LC and MS analysis were performed exactly the same as those for supernatant metabolomes. The run was performed using 50 μL of supernatant metabolite extract from the PA14 wild-type strain as the sample, 5 μL of 100 μM sodium (*R*)-2-heptyl-4,5-dihydrothiazole-4-carboxylate, sodium (*R*)-2-nonyl-4,5-dihydrothiazole-4-carboxylate, or 5 μL of 10 μM 2′-(2-hydroxyphenyl)-2′-thiazoline-4′-carboxylic acid in $CHCl_3$ as the standard, and the combination of the sample and standard as the coinjection sample.

Chrome Azurol S (CAS) Assay. CAS assay solutions were prepared exactly as previously reported in the literature (*14, 20*). For the determination of siderophore activities, 0.5 mL of CAS assay solution was added to 0.5 mL of aqueous solution of either sodium (*R*)-2-nonyl-4,5-dihydrothiazole-4-carboxylate, sodium (*R*)-2-heptyl-4,5-dihydrothiazole-4-carboxylate, HPTn-COOH, or 2,2′-bipyridyl at various concentrations, followed by an addition of 10 μL of shuttle solution. The solutions were then mixed and allowed to reach equilibrium at RT for 1 h and 45 min, before the absorbance of each solution was measured at 630 nm. The concentrations of samples used in these experiment were 5, 15, 25, and 50 μM for sodium (*R*)-2-nonyl-4,5-dihydrothiazole-4-carboxylate, sodium (*R*)-2-heptyl-4,5-dihydrothiazole-4-carboxylate, and HPTn-COOH and 5, 15, 25, 50, 150, 250, and 500 μM for 2,2′-bipyridyl. The absorbance at 630 nm of water in the mixture of CAS assay and shuttle solution was also measured as a reference (*14*). The graph was plotted as the relative absorbance at 630 nm (A_s/A_{ref}) *versus* the concentrations of samples.

Supporting Information Available: This material is available free of charge *via* the Internet at http://pubs.acs.org.

Acknowledgment: The authors would like to thank F. M. Ausubel for providing the *P. aeruginosa* mutants, C. T. Walsh for providing the PchD expression construct, and C. Reimmann for the plasmids necessary for the complementation and heterologous expression experiments. In addition, we are indebted to Michael A. Fischbach for extremely valuable discussions and guidance. This research was supported by the startup funds provided by Searle Scholar Award (A.S.), Burroughs Wellcome Fund Career Award In the Biomedical Sciences (A.S.), and funds from the Harvard University Science and Engineering Committee (N.V.).

REFERENCES

1. Walsh, C. T. (2008) The chemical versatility of natural-product assembly lines, *Acc. Chem. Res. 41*, 4–10.
2. Brady, S. F., and Clardy, J. (2005) Systematic investigation of the *Escherichia coli* metabolome for the biosynthetic origin of an isocyanide carbon atom, *Angew. Chem., Int. Ed. 44*, 7045–7048.
3. Bentley, S. D., Chater, K. F., Cerdeno-Tarraga, A. M., Challis, G. L., Thomson, N. R., James, K. D., Harris, D. E., Quail, M. A., Kieser, H., Harper, D., Bateman, A., Brown, S., Chandra, G., Chen, C. W., Collins, M., Cronin, A., Fraser, A., Goble, A., Hidalgo, J., Hornsby, T., Howarth, S., Huang, C. H., Kieser, T., Larke, L., Murphy, L., Oliver, K., O'Neil, S., Rabbinowitsch, E., Rajandream, M. A., Rutherford, K., Rutter, S., Seeger, K., Saunders, D., Sharp, S., Squares, R., Squares, S., Taylor, K., Warren, T., Wietzorrek, A., Woodward, J., Barrell, B. G., Parkhill, J., and Hopwood, D. A. (2002) Complete genome sequence of the model actinomycete *Streptomyces coelicolor* A3(2), *Nature 417*, 141–147.
4. Fischbach, M. A., Lin, H., Liu, D. R., and Walsh, C. T. (2006) How pathogenic bacteria evade mammalian sabotage in the battle for iron, *Nat. Chem. Biol. 2*, 132–138.
5. Patel, H. M., and Walsh, C. T. (2001) *In vitro* reconstitution of the *Pseudomonas aeruginosa* nonribosomal peptide synthesis of pyochelin: characterization of backbone tailoring thiazoline reductase and *N*-methyltransferase activities, *Biochemistry 40*, 9023–9031.
6. Quadri, L. E., Keating, T. A., Patel, H. M., and Walsh, C. T. (1999) Assembly of the *Pseudomonas aeruginosa* nonribosomal peptide siderophore pyochelin: *in vitro* reconstitution of aryl-4, 2-bisthiazoline synthetase activity from PchD, PchE, and PchF, *Biochemistry 38*, 14941–14954.
7. Reimmann, C., Patel, H. M., Walsh, C. T., and Haas, D. (2004) PchC thioesterase optimizes nonribosomal biosynthesis of the peptide siderophore pyochelin in *Pseudomonas aeruginosa*, *J. Bacteriol. 186*, 6367–6373.
8. Reimmann, C., Serino, L., Beyeler, M., and Haas, D. (1998) Dihydroaeruginoic acid synthetase and pyochelin synthetase, products of the pchEF genes, are induced by extracellular pyochelin in *Pseudomonas aeruginosa*, *Microbiology 144*, (11), 3135–3148.
9. Liberati, N. T., Urbach, J. M., Miyata, S., Lee, D. G., Drenkard, E., Wu, G., Villanueva, J., Wei, T., and Ausubel, F. M. (2006) An ordered, nonredundant library of *Pseudomonas aeruginosa* strain PA14 transposon insertion mutants, *Proc. Natl. Acad. Sci. U.S.A. 103*, 2833–2838.
10. Smith, C. A., Want, E. J., O'Maille, G., Abagyan, R., and Siuzdak, G. (2006) XCMS: processing mass spectrometry data for metabolite profiling using nonlinear peak alignment, matching, and identification, *Anal. Chem. 78*, 779–787.
11. Firn, R. D., and Jones, C. G. (2003) Natural products—a simple model to explain chemical diversity, *Nat. Prod. Rep. 20*, 382–391.
12. Fischbach, M. A., and Clardy, J. (2007) One pathway, many products, *Nat. Chem. Biol. 3*, 353–355.
13. Saghatelian, A., Trauger, S. A., Want, E. J., Hawkins, E. G., Siuzdak, G., and Cravatt, B. F. (2004) Assignment of endogenous substrates to enzymes by global metabolite profiling, *Biochemistry 43*, 14332–14339.
14. Schwyn, B., and Neilands, J. B. (1987) Universal chemical assay for the detection and determination of siderophores, *Anal. Biochem. 160*, 47–56.
15. Llamas, M. A., Mooij, M. J., Sparrius, M., Vandenbroucke-Grauls, C. M., Ratledge, C., and Bitter, W. (2008) Characterization of five novel *Pseudomonas aeruginosa* cell-surface signalling systems, *Mol. Microbiol. 67*, 458–472.
16. Reimmann, C., Patel, H. M., Serino, L., Barone, M., Walsh, C. T., and Haas, D. (2001) Essential PchG-dependent reduction in pyochelin biosynthesis of *Pseudomonas aeruginosa*, *J. Bacteriol. 183*, 813–820.
17. Hansen, D. B., Bumpus, S. B., Aron, Z. D., Kelleher, N. L., and Walsh, C. T. (2007) The loading module of mycosubtilin: an adenylation domain with fatty acid selectivity, *J. Am. Chem. Soc. 129*, 6366–6367.
18. Trivedi, O. A., Arora, P., Sridharan, V., Tickoo, R., Mohanty, D., and Gokhale, R. S. (2004) Enzymic activation and transfer of fatty acids as acyl-adenylates in mycobacteria, *Nature 428*, 441–445.
19. Rahme, L. G., Stevens, E. J., Wolfort, S. F., Shao, J., Tompkins, R. G., and Ausubel, F. M. (1995) Common virulence factors for bacterial pathogenicity in plants and animals, *Science 268*, 1899–1902.
20. Payne, S. M. (1994) Detection, isolation, and characterization of siderophores, *Methods Enzymol. 235*, 329–344.